

Energy demands in reinforced concrete wall piers coupled by buckling restrained braces subjected to near-fault earthquake

Hamid Beiraghi *

Department of Civil Engineering, Mahdishahr Branch, Islamic Azad University, Mahdishahr, Iran

(Received December 19, 2016, Revised September 27, 2017, Accepted April 12, 2018)

Abstract. In this study, the different energy demands in reinforced concrete (RC) wall piers, coupled by buckling restrained braces (BRBs), are investigated. As well as this, a single plastic hinge approach (SPH) and an extended plastic hinge (EPH) approach is considered for the wall piers. In the SPH approach, plasticity can extend only in the 0.1H adjacent to the wall base while, in the EPH approach, the plasticity can extend anywhere in the wall. The seismic behavior of 10-, 20- and 30-storey structures, subjected to near-fault (NF) as well as far-fault (FF) earthquakes, is studied with respect to the energy concepts involved in each storey. Different kinds of energy, including inelastic, damping, kinetic, elastic and total input energy demand, are investigated. The energy contribution from the wall piers, as well as the BRBs in each model, are studied. On average, for EPH approach, the inelastic demand portion pertaining to the BRBs for NF and FF records, is more than 60 and 80%, respectively. In the SPH approach, these ratios are 77 and 90% for the NF and FF events, respectively. It appears that utilizing the BRBs as energy dissipation members between two wall piers is an efficient concept.

Keywords: energy demand; reinforced concrete wall; buckling restrained braces; near-fault

1. Introduction

A coupled wall structure is a recognized lateral load-resisting system used for tall buildings. Traditionally, the configuration consists of two reinforced concrete (RC) shear walls connected by RC beams at each floor level. The coupling action enhances the overall system behavior by increasing the lateral stiffness and reducing the base moments pertaining to each wall pier (El-Tawil *et al.* 2010). As well as this, because of the stiffness of the RC walls, the coupling beams withstand significant ductility demands. In a design process of these systems, the purpose is to resist the seismic loads such that energy is dissipated through yielding of the coupling beams up the height of the wall, as well as through flexural yielding of the wall piers. The formation of the flexural plastic hinge at the wall base, and flexural or shear hinges at the coupling beams, is allowed in various codes (CSA Standard A23.3-04 2005, CEN EC8 2004, NZS 3101 2006).

As the coupling beams are subjected to inelastic deformations during a severe event, they dissipate seismic energy. Therefore, the large deformation associated with the plastic hinges at the bases of the walls is reduced when compared to the cantilever RC walls (Harries and McNeice 2006). The plasticity is distributed over a more extensive area of the structure, with considerably higher energy dissipation compared to the energy dissipation of the cantilever RC walls (Harries *et al.* 2000).

The specifications of ground motions in the vicinity of

an active fault are significantly different from those of far-fault (FF) earthquakes. This issue severely affects the damage potential of these ground motions (Gerami and Sivandi-Pour 2014, Beiraghi 2017a). Near-fault (NF) seismic ground motions have frequently features like intense velocity and displacement pulses of relatively long period that clearly distinguish them from typical far-fault earthquakes (Stewart *et al.* 2001). The study of outstanding effects of near-field ground motions versus far-field records leads to gaining a better perception about the seismic responses of structures. Forward directivity phenomena is an important characteristic of near-fault events. Usually, when evaluating the earth's movement for a near-fault zone, these special properties of near-fault earthquakes are considered. Near-fault motions can cause significant damage during a strong ground motion, especially to structures, with natural periods close to those of the motion pulse (Somerville 1997, Baker *et al.* 2007). The Near-fault motion specification depends on the shaking intensity, fault geometry and the orientation of the strong motion waves (Mortezaei and Ronagh 2013, Beiraghi *et al.* 2016a).

Energy demand is assumed to be a reliable tool for the prediction of seismic hazards. In recent years, researchers have focused on various energy concepts in the field of earthquake engineering, in such a way that the energy concept is used in the optimized design and vulnerability evaluation of buildings under strong ground motion. The hysteretic energy input is an important parameter involved in the investigation of seismic responses of structures subjected to seismic loadings.

The energy input of structures, resulting from strong ground motions, has been measured by some researchers (Uang and Bertero 1997, Kuwamura and Galambos 1989,

*Corresponding author, Ph.D.,
E-mail: h.beiraghi@msh-iau.ac.ir

Kalkan and Kunnath 2007, 2008, Beiraghi 2017b). These studies demonstrated the possibility of hysteretic energy input as a good parameter for recognizing structural demands and damages.

Near-fault motions have special properties that cause a structure to dissipate earthquake input energy in a number of large plastic cycles. It appears that the study of energy demand in structures and its distribution, as well as the investigation of structural properties, leads to a more precise understanding of seismic responses in earthquakes (Kalkan and Kunnath 2006, Beiraghi *et al.* 2016b). Earthquake input energy is a useful intensity measure for near-fault types of ground motions (Luco and Cornell 2007). This parameter accounts not only for the ground motion specification, such as duration or frequency content of motions, but also for structural properties such as ductility, damping, and hysteretic behavior.

BRBs are recognized structural elements that have a considerable energy dissipation capability. In fact, BRBs are relatively new braces that can prevent the phenomenon of buckling in compression compared to conventional braces. They are designed to yield and dissipate energy in both tension and compression action (Black *et al.* 2002, Abdollahzadeh and Banihashemi 2013). In conventional steel braces, the buckling of braces reduces the efficiency of the element in compression, while the hysteretic behavior of braces deteriorates severely under strong cyclic loads. In the BRBs, the basic idea is to confine a steel core element so that it can yield in compression as well as tension. Concrete-filled steel tubes are used to provide confinement for the steel core. Significant energy dissipation and ductility by BRBs has been demonstrated by experiments (Watanabe 1992). Several experimental and numerical researches have investigated the seismic performance of the frames with BRBs (Fahnestock *et al.* 2007, Tsai *et al.* 2008, Tsai and Hsiao 2008, Palmer *et al.* 2014). These researches identified the advantages of BRBFs, e.g., ductility and energy dissipation capability, up to and beyond the expected design-level earthquake demands.

In general, having plasticity near the base of the wall is preferable in the cantilever RC walls (Paulay and Priestley 1992). In this approach, known as SPH (single plastic hinge) approach in this paper, plasticity can extend only to $0.1H$ adjacent to the wall base. Another approach, in which plasticity can extend anywhere in the wall, is called EPH (extended plastic hinge) approach. In this paper, the different energy demands in the RC wall pier coupled by BRBs are investigated. As well as this, the SPH approach and EPH approach is considered for the wall piers. The seismic behavior of 10-, 20- and 30-storey structures that were subjected to NF and FF records is studied with respect to the energy concepts. Figure 1 presents the SPH and EPH concept used in this study. The different kinds of energy and the energy contribution from wall piers, as well as BRBs, in each model are studied. The portion of each set of walls and BRBs is determined by the inelastic energy dissipated in the whole proposed system. It should be noted that in construction industry, the connection of a steel beam to a wall may be carried out by special details. This subject is beyond the current paper and the interested readers may refer to proper resources.

2. Design of the systems

The 10-, 20- and 30-storey wall piers, coupled by BRBs with fixed bases and with a typical storey height of 3.5 m, are considered here in this research. For design purposes, a two-dimensional linear elastic finite element model of the core wall was generated in ETABS software (version 13.1.1). In this computer program, the shell-type plate elements were used to simulate the shear wall. The wall thickness was constant along the height. Fig. 1 plots the general view of the assumed structures. Line elements were used to model the beams, which were made of steel. The

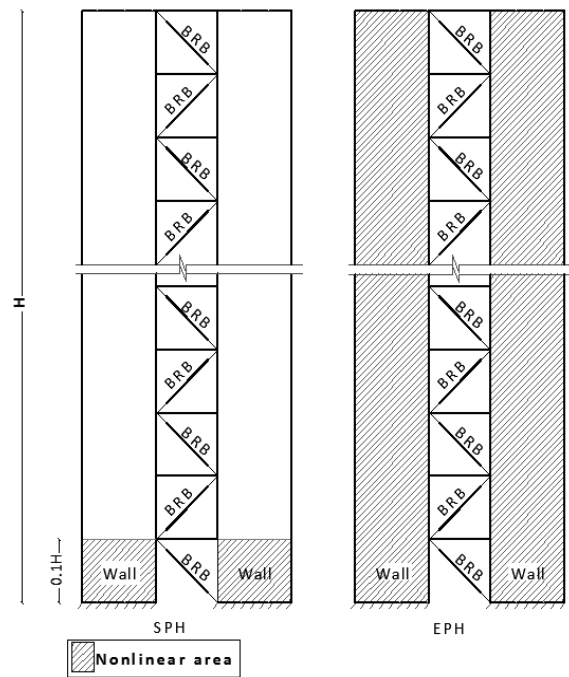


Fig. 1 Single plastic hinge and extended plastic hinge approach for the considered systems

Table 1 Specification of designed system

	10 ST	20 ST	30 ST	
Seismic weight pertaining to the building, W (ton)	1710	6040	15900	
$P/(A_g f_c)$ at the wall base	0.056	0.078	0.097	
Wall thickness (cm)	60	75	110	
Horizontal length of each wall (m)	3	4.5	6.5	
Design base shear/ W (%)	11.8	6.9	6.0	
Final response modification factor used in RSA (R or R_{eff})	5	5	4.56	
Period of natural vibration	T1	0.89	2.23	3.38
	T2	0.235	0.49	0.68
	T3	0.109	0.22	0.31
Modal participation mass ratio for mode No.	1	69	65	64
	2	17	19	19.5
	3	5.5	6	6
	4	3	3	3.2

nominal design yielding stress of the rebar and steel material of the beams were 400 and 370 MPa, respectively. The nominal strength of the compression concrete was 45 MPa. The connection of beam and brace to wall was of the pinned type. In each storey, the dead and live load portion carried by the wall were assigned to the wall. The mass portion of each storey was assigned to the mass center of the storey. The design of the systems was based on the ASCE-7 and ACI318-11 (ACI 318-11 2011, ASCE/SEI 7-2010 2010). The specifications of the designed systems are shown in Tables 1 and 2. The vertical steel reinforcement distribution was uniform at each cross-section. The reinforcement ratio of the wall and BRB specification was identical in every 0.2H. The minimum vertical reinforcement ratio was 0.25% (ASCE/SEI 7-2010 2010). The calculated vertical reinforcement ratio in the wall pier is shown in Table 2. In order to obtain the effective moment of inertia, a coefficient of 0.5 was used for the gross moment of inertia of the wall. This coefficient is in accordance with the stiffness reduction factors recommended in ACI 318-11 (Sections 8.8 and 10.10). The reduction coefficient was used for the effective moment of inertia of the RC wall cross-sections.

The natural free vibration periods, mode shapes and modal mass participation factors were determined using the eigenvalue analysis. More than 97% of the modal participation mass ratio corresponded to the first five translational modes of vibration. A 5% damping DBE level response spectrum was used in the RSA procedure (see Fig. 2). The walls were assumed to remain together with a framing system, in which the ordinary reinforced concrete shear walls were used. A response modification factor equal to five ($R = 5$) was used to calculate the design demand from equivalent static procedure (ASCE/SEI 7-2010 2010). The base shear force resulting from elastic RSA, namely V_t , was modified so that its quantity equaled 0.85 times the design equivalent static base shear force, V . ASCE 7 requires the forces to be multiplied by 0.85 V/V_t (ASCE/SEI 7-2010 2010), when the combined modal base shear demand is reduced by dividing by a design R factor (V_t) and is less than 85% of the design equivalent static base shear force (V). This matter controlled the 30-storey building; therefore, the effective response modification

Table 2 Wall longitudinal reinforcement and cross-section area of the BRBs

Height range	Vertical rebar ratio of wall (%)			Core cross-section area of BRB (cm ²)		
	10ST	20 ST	30ST	10ST	20 ST	30ST
0-20%	2.24	2.34	2.22	88	150	300
21-40%	1.3	1.39	1.29	88	140	230
41-60%	0.87	1.05	1.01	88	100	140
61-80%	0.56	0.77	0.79	75	88	120
81-100%	0.32	0.34	0.38	47	75	100

factor in the RSA procedure, R_{eff} , is less than 5. To calculate the size of BRB braces, axial forces calculated from the modal response spectrum analysis were reduced by the value of the response modification factor. The capacity of the braces in tension and compression were considered as $\phi A F_y$, where A is the cross-section of the brace element, $\phi = 0.9$ and $F_y = 250$ MPa (Sahoo and Chao 2010). Except for their nonlinear model, SPH and EPH have similar design procedures. While the whole wall has the ability to experience inelastic behavior in nonlinear model of EPH, in SPH only the 0.1 H is able to experience plasticity and the upper regions are essentially elastic.

3. Nonlinear modeling

Perform-3D software was used to implement the nonlinear time history analysis (NLTHA) and to calculate the responses (PERFORM-3D, 2011). Fiber elements used for the RC wall modeling. The cross-section of the wall model contained steel and concrete fibers. For the nonlinear fiber model of the wall, a confined concrete stress-strain based on the modified Mander model was assumed (Mander *et al.* 1988). Tensile strength of the concrete was ignored.

In each storey, a single wall element was used to model each wall pier (PERFORM-3D User Guide 2006). The expected material strength was in accordance with the recommendations of the references; for this purpose, the compressive strength of concrete was 1.3 times the

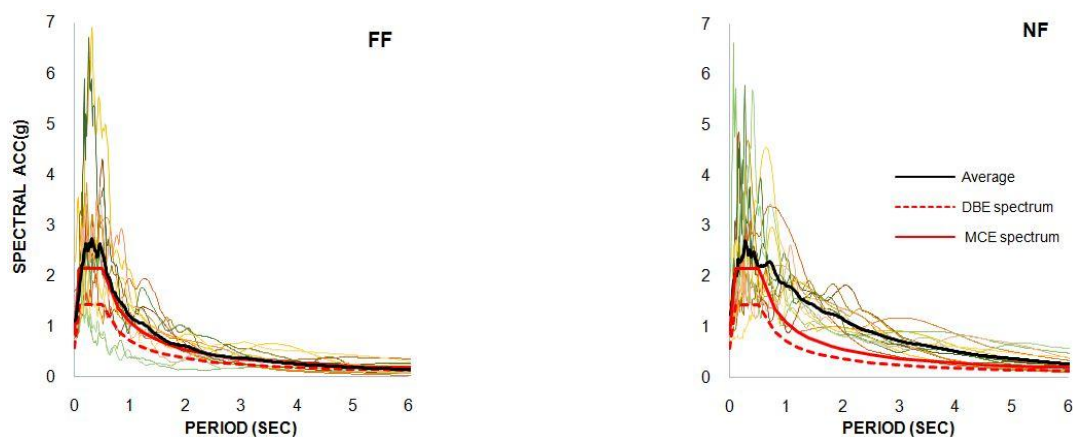


Fig. 2 DBE, MCE, individual and average spectra

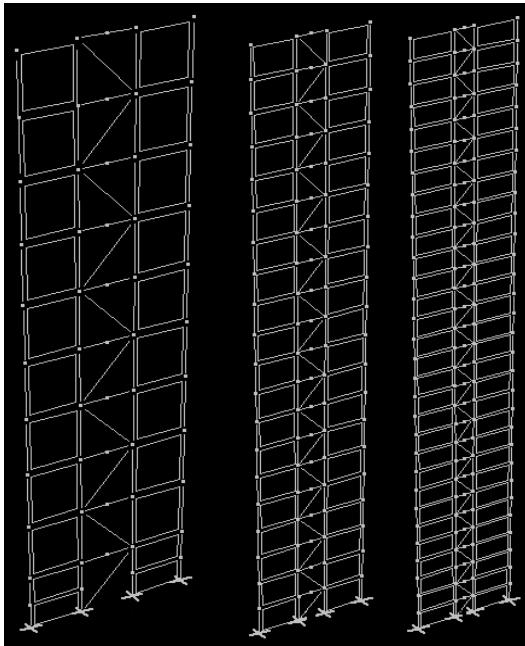


Fig. 3 Numerical nonlinear model of the considered structures

specified design strength used in the design procedure, while the rebar yield strength was taken at 1.17 times its nominal yield strength, according to LATBSDC (2011). Degradation of the strength and stiffness was considered by the degradation factor for longitudinal reinforcements. This factor accounts for the ratio of the areas of the degraded to non-degraded hysteresis loops (Ghods and Ruiz 2010). The beams were modeled with elastic elements. The mass of each storey was assigned to its center of the mass, while a rigid diaphragm was used to equalize the horizontal displacement of the nodes of each floor. In the fiber element method, it is important to use the effective plastic hinge length at the base of the wall models. The plastic hinge length (L_p) in the RC walls can be calculated from the following equation given by Paulay and Priestley (1992)

$$L_p = 0.2L_w + 0.03H \quad (1)$$

Where L_w is the RC wall length and H is the wall height. The height of the wall element used to model the plastic hinge region shall not exceed the length, L_p , or the storey height at the location of the critical section (LATBSDC 2011). Fig. 3 plots the elevation view of the nonlinear structural models. In the EPH approach, all the wall elements along the height can experience nonlinear behavior. In the SPH approach, only 0.1 H of the wall adjacent to the base can experience nonlinear behavior and, for the upper levels, the elastic wall element is used (Panagiotou and Restrepo 2009, Beiraghi and Siahpolo 2016). In order to take the crack effect on flexural stiffness of the elastic elements into consideration, a coefficient of 0.5 is used. For all the wall elements, a linear response was assumed for the shear action. For RC wall simulation, one element per storey has been recommended by Powell (2007).

The post-yield stiffness of BRBs in the tension is

different from that in compression. The reason for this is the Poisson expansion effect and friction at the interface between the steel core and the surrounding material. According to the AISC Seismic Provisions, the real compression behavior of BRBs and strain-hardening effect is accounted for by using the adjustment factors. Thus, the maximum compression forces from the brace are calculated as $R_y \omega \beta A F_y$, where $R_y = 1.1$ accounts for the material over strength, $\omega = 1.25$ considers the strain-hardening effect and $\beta = 1.1$ is the compression over-strength factor (Jones and Zareian 2013).

The BRB element in the Perform-3D is a line type element that resists axial force only and has no resistance to torsional or bending forces (PERFORM-3D User guide 2006). The element contains two portions in series: a linear portion that is elastic, and a nonlinear core portion that is capable of yielding. The length of the restrained nonlinear core portion of a BRB element was assumed to be 0.7 of the node-to-node brace element length. The remaining 30% was considered as the linear non-yielding portion. This linear portion of the brace accounts for the stiffness of the gusset, the brace connection, and the portion of the column that is not considered in the center-line to center-line geometry. Commonly, the linear portion includes a transition segment and an end segment (Fig. 4). To prevent the yielding of the transition and end segments, the cross-section areas of these segments are considered larger than the restrained nonlinear core portion. In this study, the cross-section area of transition and end segments (A_t and A_e) of the BRB elements were chosen as 1.6 and 2.2 times the area of the core cross-section area, respectively. Furthermore, the length of the transition and end segments were chosen as 0.06 and 0.24 times the total length of the bracing, respectively (Nguyen *et al.* 2010). To calculate the cross-section area of the nonlinear core (A_c) of the BRB element, the following equation was used

$$\frac{L_c}{A_c} = \frac{L_w}{A} - \frac{L_e}{A_e} - \frac{L_t}{A_t} \quad (2)$$

Where L_c , L_t , L_e and L_w represent the lengths of the yielding core, transition segment, end segment and the whole bracing, respectively; and where A is the cross-section area of the equivalent bar calculated from the linear design procedure. Fig. 5 plots the general view of the backbone curve for the BRB element used in the nonlinear model (Simpson *et al.* 2009).

The damping assumption is known to severely affect the behavior of the structure that is subjected to NLTHA (Priestley and Grant 2005).

Some researchers believe that the use of Rayleigh damping may cause large, unrealistic damping forces (Bernal 1994, Sivandi-Pour *et al.* 2015). Chopra (2001) states that Rayleigh damping can only be used in a structure in which proper damping mechanisms are provided throughout the system. Perform-3D software has the capability to implement Rayleigh damping as well as modal damping. The software user guide recommends that a small amount of Rayleigh damping should be combined with modal damping (Perform-3D User Guide 2006). This

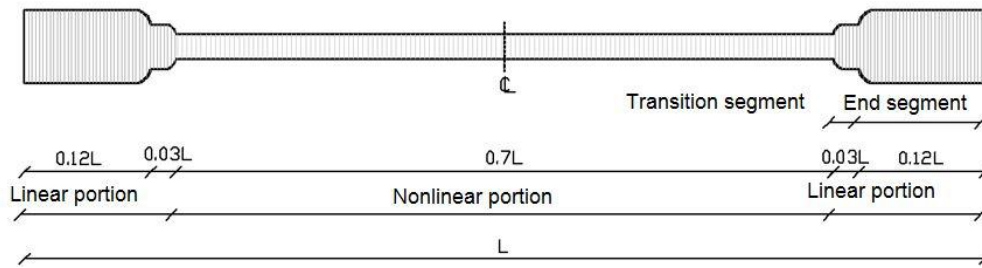


Fig. 4 Linear and nonlinear portion pertaining to the buckling restrained brace

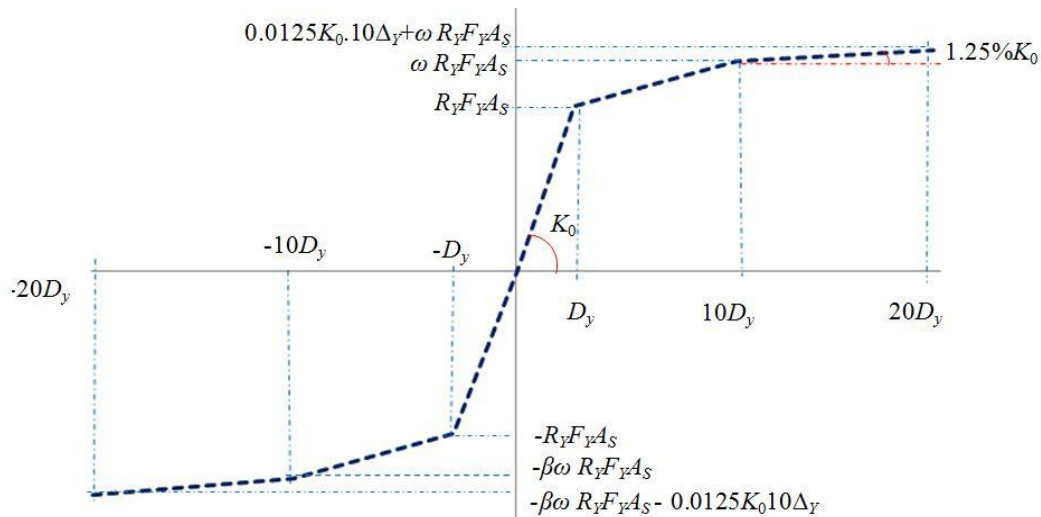


Fig. 5 Backbone curve used in the nonlinear model of the BRB (Ghodsi and Ruiz 2010)

approach was used to damp out high-frequency vibrations. In order to use the Rayleigh damping, a two-mode number is required. It is common to select the first mode and the mode for which the accumulated modal mass participation is larger than 90% of the total mass. In this research, 2.5% of the modal damping for all modes of vibration, alongside 0.15% Rayleigh damping for the first and third modes, were used (Perform-3D User Guide 2006).

4. Software verification

Various researchers have demonstrated the capability of the fiber element models to simulate the behavior of RC shear walls and the interested readers may refer to proper resources (Beiraghi *et al.* 2015, Orakcal and Wallace 2006). To study the performance of the BRB elements in the Perform-3D software, specification and results from an experimental test performed by Merritt *et al.* (2003) were used. Fig. 6 compares the force-displacement hysteretic response from the numerical and experimental tests. The overall curves obtained from the numerical model and test program were roughly similar.

5. Accelerograms

Scaling method is important for NLTHA (Beiraghi *et al.* 2016c). For this research, a set of 14 horizontal near-fault

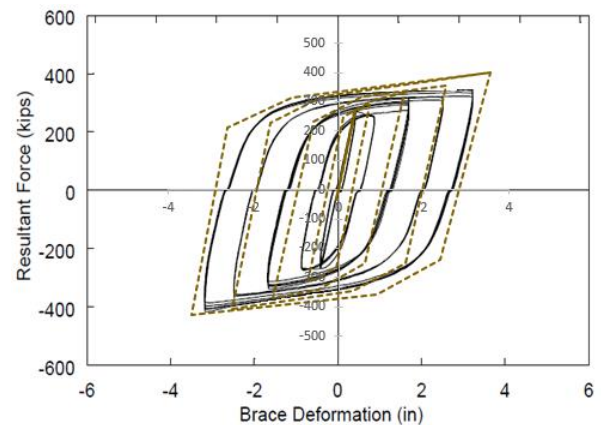


Fig. 6 Hysteretic graph corresponding to the BRB obtained from numerical model (dashed lines) and experimental test of Merritt *et al.* (2003)

pulse-like and 14 far-fault ground motion records were selected from the events given in Table A-6A and Table A-4A of the FEMA P695 (2009), respectively. The time-histories of the earthquakes were obtained from the PEER NGA database. Fault normal components of the records were used in the NLTHA. The characteristics of the strong ground motions are presented in Table 3. The maximum considered earthquake (MCE) level was used to scale the records. The spectrum curve corresponding to the MCE level was 1.5 times the response spectrum curve for DBE

Table 3 List of ground motion specification used to carry out nonlinear analysis

	Event name	Year	Station	Duration(s)	PGA*	PGV**	<i>M</i>	Site-to-source distance (km)***
Near-fault record	Imperial valley-06	1979	El centro Array#6	39	0.44	111.9	6.5	1.4
	Imperial valley-06	1979	El centro Array#7	37	0.46	108.9	6.5	0.6
	Irpinia. Italy-01	1980	Sturno	40	0.31	45.5	6.9	10.8
	Superstition-hills-02	1987	Parachute test site	22.3	0.42	106.8	6.5	1.0
	Loma Prieta	1989	Saratoga-Aloha	40	0.38	55.6	6.9	8.5
	Erizican-Turkey	1992	Erizican	20.8	0.49	95.5	6.7	4.4
	Cape Mendocino	1992	Petrolia	36	0.63	82.1	7	8.2
	Landers	1992	Lucerne	48	0.79	140.3	7.3	2.2
	Northridge-01	1994	Rinaldi Receiving Sta	20	0.87	167.3	6.7	6.5
	Northridge-01	1994	Sylmar-Olive View	40	0.73	122.8	6.7	5.3
	Kocaeli/IZT	1999	Izmit	30	0.22	29.8	7.5	7.2
	Chi chi, Taiwan	1999	TCU065	90	0.82	127.7	7.6	0.6
	Chi chi, Taiwan	1999	TCU102	90	0.29	106.6	7.6	1.5
	Duzce	1999	Duzce	26	0.52	79.3	7.1	6.6
Far-fault record	Northridge	1994	Canyon Country-WLC	20	0.48	45	6.7	12.2
	Duzce	1999	Bolu	56	0.82	0.62	7.1	12.0
	Hector Mine	1999	Hector	45.3	0.34	42	7.1	11.7
	Imperial valley	1979	Delta	100	0.35	33	6.5	22
	Imperial valley	1979	El centro Array#11	39	0.38	42	6.5	12.5
	Kobe, Japan	1995	Shin- Osaka	41	0.24	38	6.9	19.2
	Kocaeli, Turkey	1999	Duzce	27.2	0.36	59	7.5	15.4
	Kocaeli, Turkey	1999	Arcelik	30	0.22	40	7.5	13.5
	Landers	1992	Yermo Fire Station	44	0.24	52	7.3	23.6
	Loma Prieta	1989	Gilroy Array	40	0.56	45	6.9	12.8
	Superstition Hills	1987	El Centro Imp. Co.	40	0.36	46	6.5	18.2
	Superstition Hills	1987	Poe Road (temp)	22.3	0.45	36	6.5	11.2
	Chi chi, Taiwan	1999	Chy101	90	0.44	115	7.6	10
	San Fernando	1971	LA-Hollywood Stor	28	0.21	19	6.6	22.8

* PGA: Peak ground acceleration; ** PGV: Peak ground velocity; *** This is epicentral

level. The assumed class for the site was *C* and accelerograms were scaled such that the average 5% damped spectrum curve for the periods ranged from $0.2 T$ to $1.5 T$, located above the MCE spectrum, where T is the first mode period of the natural vibration (ASCE/SEI 7-2010 2010). The resulted scaled spectra for the near-fault and far-fault motions are presented in Fig. 2.

6. Energy methodology

Generally, to perform a dynamic analysis of multistorey structures, the following equation of motion is used (Chopra 2001)

$$\mathbf{M} \cdot \ddot{\mathbf{u}} + \mathbf{C} \cdot \dot{\mathbf{u}} + \mathbf{K} \cdot \mathbf{u} = -\mathbf{M} \cdot \mathbf{r} \cdot \ddot{\mathbf{u}}_g(t) \quad (3)$$

where \mathbf{M} is the mass matrix, \mathbf{C} accounts for the damping

matrix, \mathbf{K} considers the stiffness force, \mathbf{u} represents the relative displacement vector of the degrees of freedom, $\dot{\mathbf{u}}$ and $\ddot{\mathbf{u}}$ is the relative velocity of the degrees of freedom, \mathbf{r} is the influence vector (the matrix of influence coefficients), and $\ddot{\mathbf{u}}_g$ is the ground acceleration. During a strong ground motion, depending on the site, structure, and the earthquake specifications, such as frequency contents of the records, the structures endure different levels of earthquake energy. Due to the transferred energy to the structure by the rare events, the responses in the structure lead to elastic and inelastic deformations in the structural elements. By multiplying Eq. (3) by the transposed velocity term, and then integrating it over the time duration of the ground motion, the following equation is obtained

$$\int_0^t \dot{\mathbf{u}}^T \mathbf{M} \ddot{\mathbf{u}} dt + \int_0^t \dot{\mathbf{u}}^T \mathbf{C} \dot{\mathbf{u}} dt + \int_0^t \dot{\mathbf{u}}^T \mathbf{K} \mathbf{u} dt \quad (4)$$

$$= - \int_0^t \mathbf{u}^T \mathbf{M} \mathbf{r} \ddot{u}_g dt \tag{4}$$

$$E_k + E_d + (E_{el} + E_{ine}) = E_i \tag{5}$$

$$E_{el} + E_{ine} = \int_0^t \mathbf{u}^T \mathbf{K} \mathbf{u} dt \tag{6}$$

Where t represents the time. In the Eq. (4), from left, the first term is the kinetic energy corresponding to the masses E_k , the second term is the energy dissipated by the damping influence E_d , and the third term is the internal work or energy absorbed by the structural members, which are comprised of elastic E_{el} and inelastic (hysteresis) energy, E_{ine} . Structural damage occurs when the deformations enter the inelastic range. The right term is the total relative input energy E_i . Eq. (5) summarizes the energy equilibrium equation described above. This equation illustrates that the

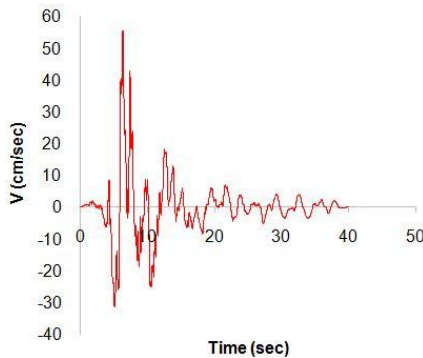
input energy imposed on the structure by the earthquake, is equal to the four other energies related to the structural properties at any time.

Energy can be expressed via the equivalent velocity. For each kind of energy demand, the equivalent velocity (V_e) is a measure of energy that is related to energy (E) and seismic mass (M). It can be obtained from $V_e = \left(\frac{2E}{M}\right)^{0.5}$.

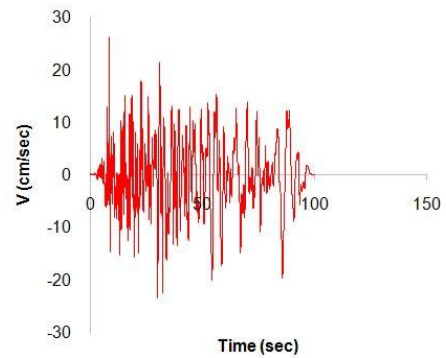
7. Results

7.1 Input energy

Ground motion velocity time-history for a sample NF and a sample FF earthquake has been compared in Fig. 7. After completing the NLTHA, different kinds of energy were calculated for all the records. Fig. 8 plots various kinds of energy during one sample FF and one sample NF



(a) NF Saratoga-Aloha station of the Loma Prieta earthquake



(b) FF Delta station of the Imperial Valley earthquake

Fig. 7 Ground motion velocity time-history for the sample (a) NF; and (b) FF earthquakes

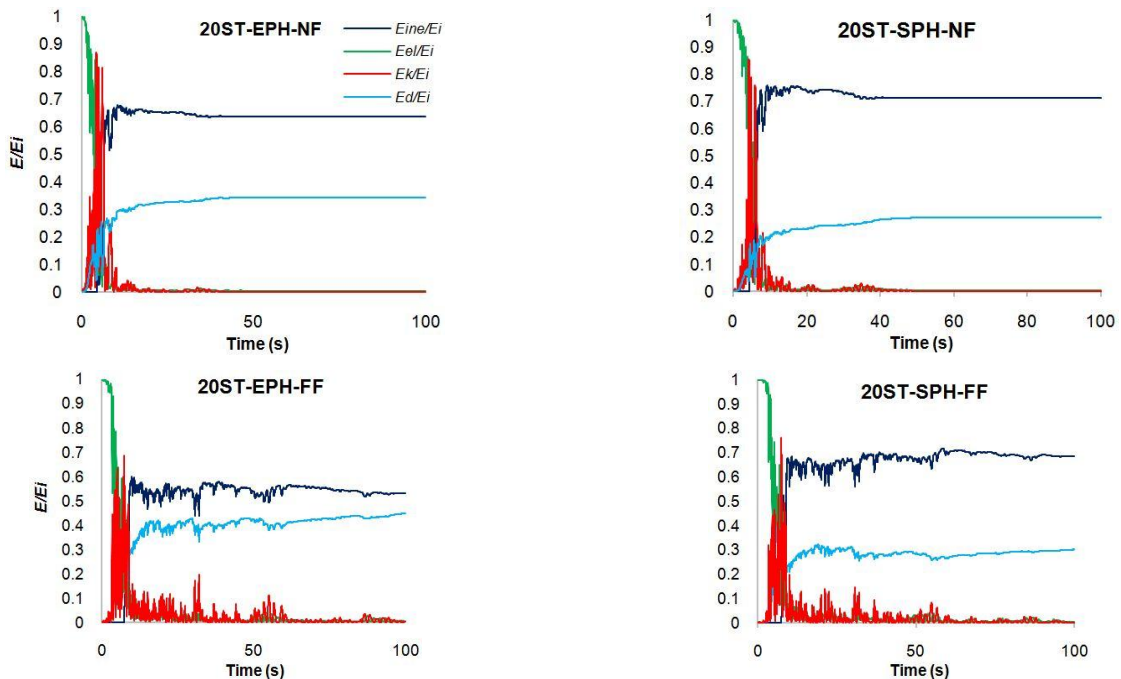


Fig. 8 The ratio of E_{ine}/E_i , E_d/E_i , E_{el}/E_i and E_k/E_i during sample NF and FF earthquakes pertaining to the 20-story structure

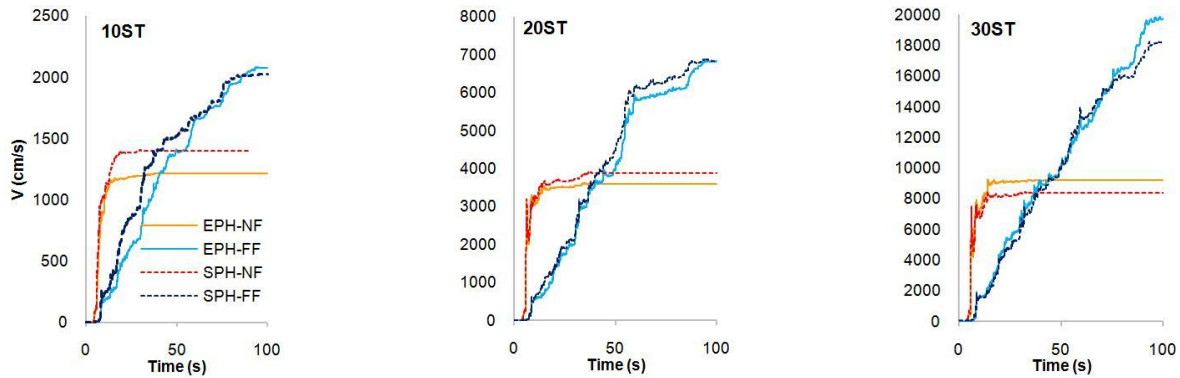


Fig. 9 Input energy pertaining to the 20-storey-SPH and -EPH subjected to the sample NF and FF earthquakes

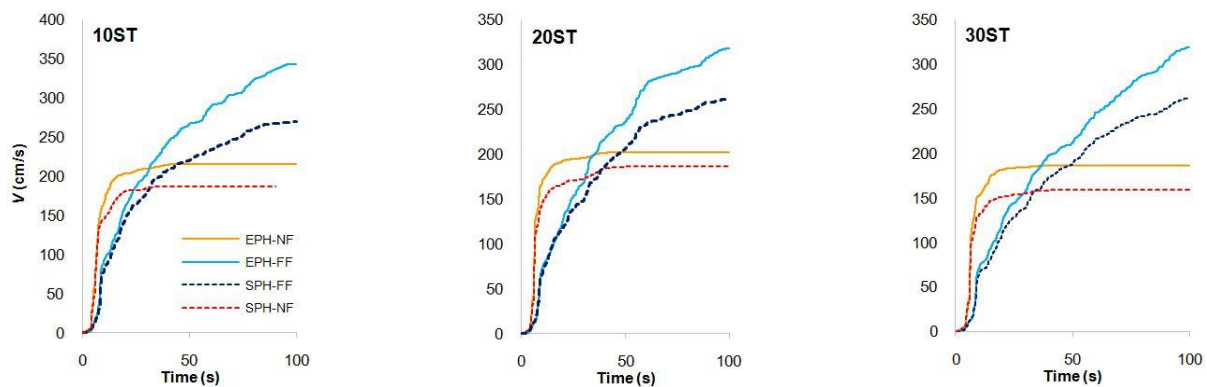


Fig. 10 Accumulative damping energy pertaining to the 20-storey-SPH and -EPH subjected to the sample NF and FF earthquakes

ground motion for the EPH and SPH approaches, corresponding to the 20-storey building. Each kind of energy was normalized by dividing it by the E_i . The Delta of the Imperial Valley earthquake is used as a sample FF event and the Saratoga-Aloha station of the Loma Prieta earthquake is used as a sample NF event. Fig. 8 shows that the time-histories of the E_k/E_i and E_{el}/E_i ratios can contain variable quantities and large oscillations during the earthquakes. When the structure vibrates in linear range, this issue is more significant and is more intense for the NF records. The large ratios of E_k/E_i and E_{el}/E_i disappear rapidly as the systems experience inelastic deformation.

This means that a large portion of the input energy is converted to inelastic (hysteretic), as well as damping energies, rather than the kinetic and elastic strain energies. The general trend of the 10- and 30-storey systems are similar to the 20-storey system, but which has not been represented here.

For both the SPH and EPH approach, Fig. 9 compares the input energy that is subjected to the sample FF and NF events during the ground motions. The vertical axis represents the equivalent velocity. For the NF events, there is a rapid increase in the input energy curves that does not occur in the FF events. When comparing Fig. 9 with Fig. 7,

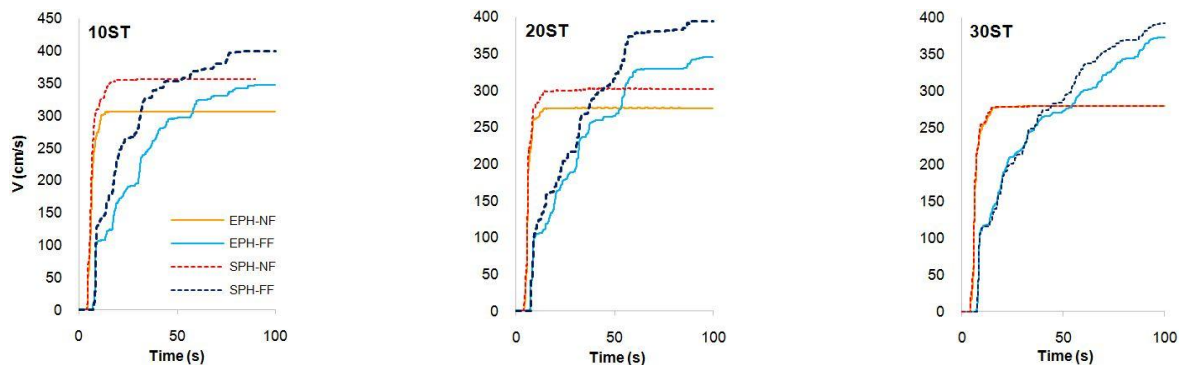


Fig. 11 Accumulative inelastic energy pertaining to the 20-storey-SPH and -EPH subjected to the sample NF and FF earthquakes

it is understood that the quick rise in the input energy coincides with the arrival of the forward directivity pulse in the NF earthquakes. Generally, this issue is also true for the other selected records in this paper, which have not been presented here. The general trend for the input energy graph pertaining to the SPH approach is similar to the EPH approach. However, there is not a general rule to say which one has a greater input energy, while this matter depends on the earthquake characteristics as well as the structural specifications.

7.2 Sample for damping, inelastic, kinetic and elastic energy

Fig. 10 shows the accumulated damping energy in equivalent velocity form during the sample FF and NF events corresponding to the 10-, 20- and 30-storey building for sample earthquakes. The general difference between the NF and FF events is similar to the input energy mentioned previously. Generally, the damping curve from the EPH approach is larger than the damping curve from the SPH approach. One reason for this is the modal damping process and other assumptions in the software. In the modal damping procedure for a linear structure, each mode is independently damped. In the software, this matter is extended to a nonlinear structure. In the modal damping process for a nonlinear structure, it is assumed that the damping matrix remains constant. At any instant of time, the deformed shape of the system still contains contributions from the elastic mode shapes. However, unlike the linear deformation, the effective periods of vibration for these shapes are not identical to the linear periods, while the shapes are generally not independent (uncoupled). Also, the deformed shape contains shapes other than the linear mode shapes. Therefore, the only

components of the deformed shape that are damped are those that correspond to the linear mode shapes. All other deformations are undamped. Indeed, this type of model is probably the best that is currently available (PERFORM-3D User Guide 2006).

Fig. 11 shows the accumulated dissipated inelastic energy in the equivalent velocity term during the sample of FF and NF events corresponding to the considered structures. On average, during the research it was found that the time duration at which almost 90% of the input inelastic energy occurs, when subjected to the FF events, is greater than approximately 4 times the length of time at which the same percentage of the input inelastic energy occurs, when subjected to the NF events. For the NF events, there is a rapid increment in the inelastic energy demand curve; this issue does not occur for the FF events.

Fig. 12 shows the time history of kinetic energy for the SPH and EPH approach during the sample FF and NF events corresponding to the 10-, 20- and 30-storey systems. The maximum kinetic energy belongs to the NF event; this is because of the pulse effect in the time history in the sample NF record.

Fig. 13 shows the time history of the elastic strain energy in the form of equivalent velocity corresponding to the SPH and EPH approaches, subjected to the sample FF and NF earthquakes. As can be seen, large amounts of the elastic strain energy are exerted on the structures by the arrival time of the NF forward directivity pulse. After stopping the vibration, there is residual deformation and, therefore, residual energy in the systems.

7.3 Average inelastic, damping and total input energy

Fig. 14 shows the average inelastic, damping and total



Fig. 12 Kinetic energy pertaining to the 20-storey-SPH and -EPH subjected to sample the NF and FF earthquakes



Fig. 13 Elastic energy pertaining to the 20-storey-SPH and -EPH subjected to the sample NF and FF earthquakes

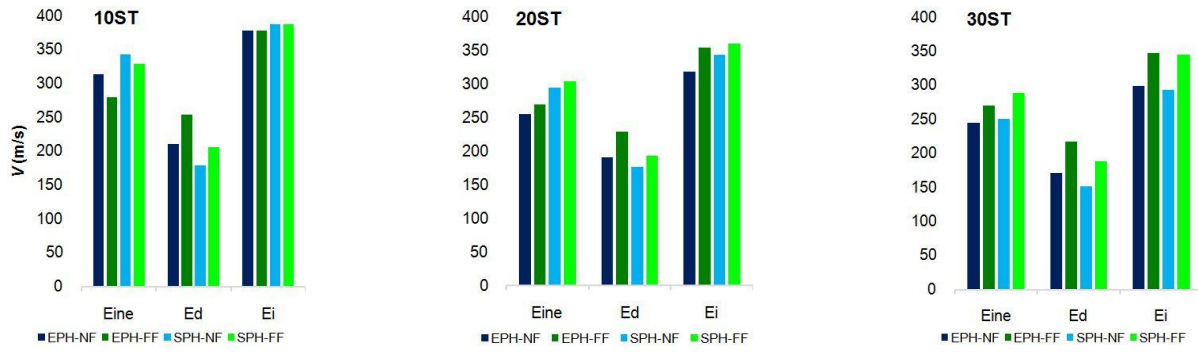


Fig. 14 Average total input, inelastic and damping energy at the end of the oscillation obtained from the all NF and FF record sets

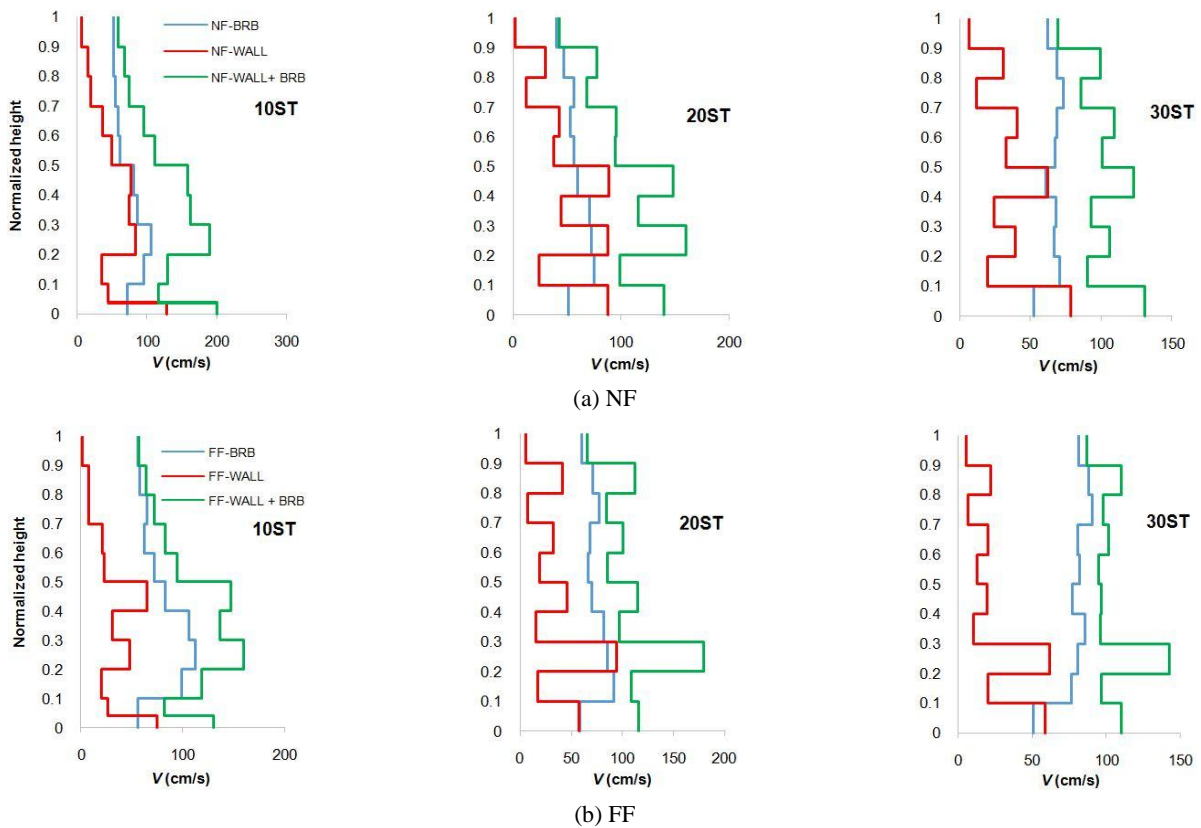


Fig. 15 Distribution of average inelastic energy demand along the height of the EPH models subjected to all the NF and FF record sets

input energy in the form of equivalent velocity obtained from 14 FF and 14 NF event sets at the end of the oscillations, corresponding to the SPH and EPH approaches. In each of the FF and NF cases, the difference between the various kind of energy values obtained from the SPH and EPH approaches is not very significant. On average, the input energy quantity from the NF records is less than the corresponding values from the FF records. For example, for the 20-storey-EPH approach, the average input energy from the FF events is almost 1.1 times the average input energy from the NF events, the coefficient of which is 1.05 for the 20-storey-SPH approach. Commonly for the taller buildings of the SPH approach, the FF events cause more input energy exertion compared to the NF events. This

matter is related to the specification of the records and the structures. Generally, SPH approach shows larger inelastic energy dissipation compared to the EPH approach. The reason is greater participation of the BRBs in the SPH approach compared to the EPH approach.

Fig. 15 plots the distribution of average inelastic energy demand along the height of the EPH models subjected to all NF and FF record sets. Furthermore, in each level, it shows the contribution of wall piers and BRBs. It is evident that, in almost all cases (except the 30-storey-NF), the maximum inelastic energy demand occurs around 0.3 H. In some of the wall piers, the inelastic energy dissipation in the upper region exceeds the corresponding values at the base. Furthermore, near the base level, the inelastic energy

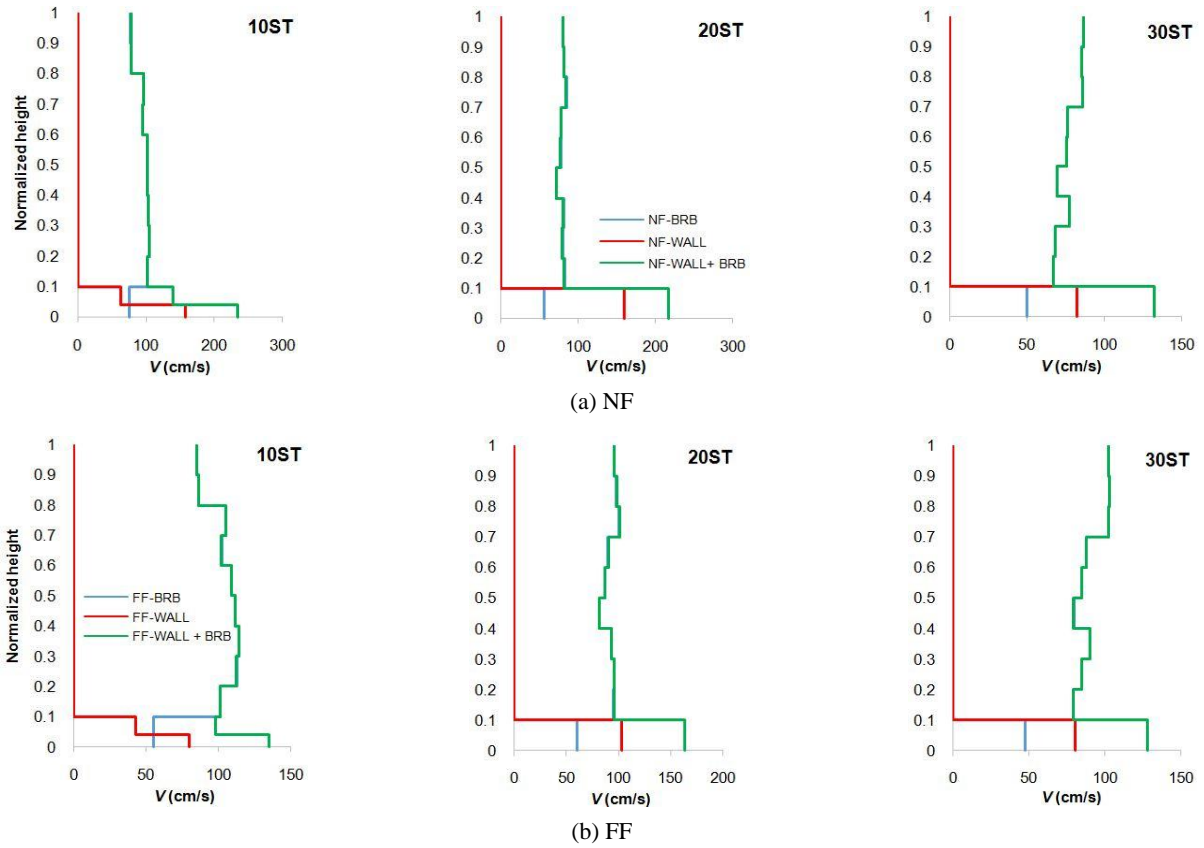


Fig. 16 Distribution of average inelastic energy demand along the height of the SPH models subjected to all the NF and FF record sets

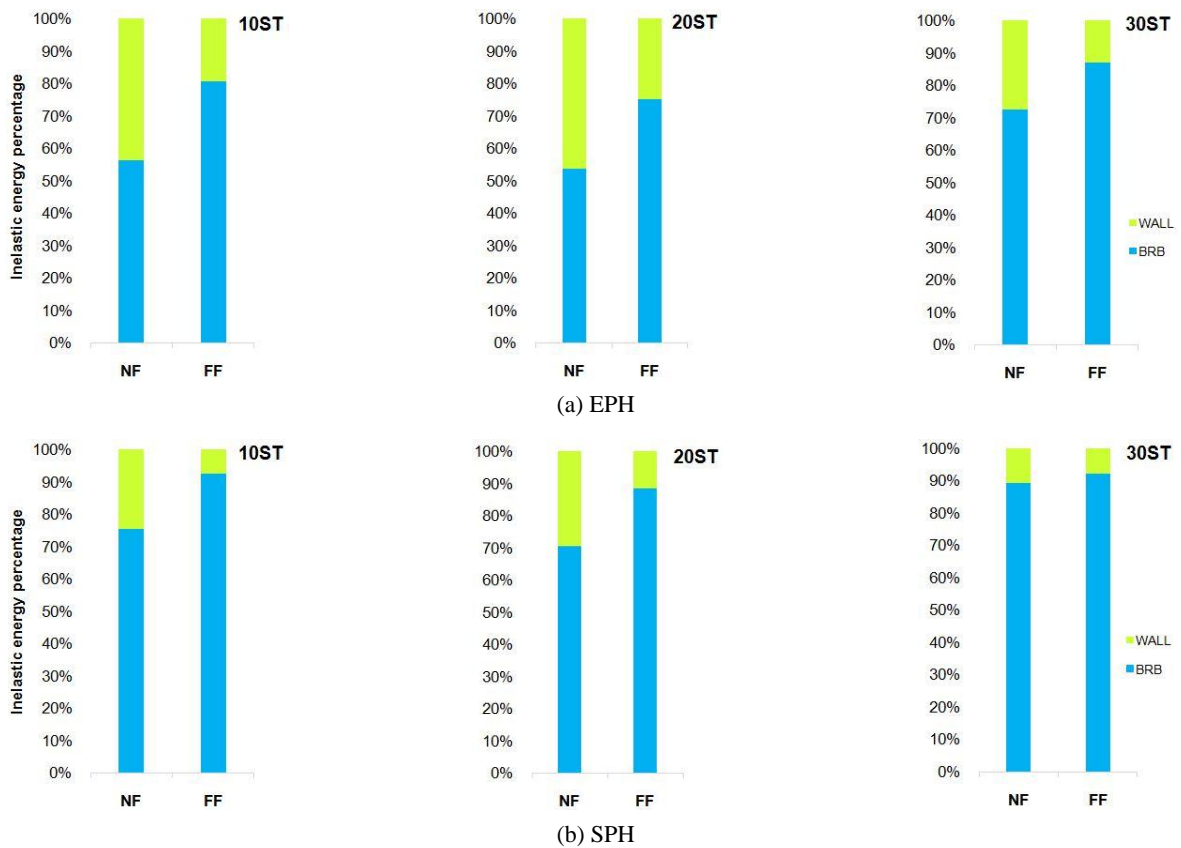


Fig. 17 Contribution of wall pier sets and the whole BRBs in the inelastic energy obtained from 14 FF and 14 NF event sets

dissipation portion from the wall pier is larger than the corresponding portion from the BRBs. This issue is generally reversed at the upper levels; however, there are exceptions. Fig. 16 shows similar graphs for the SPH approach. In the 0.1 H adjacent to the base level, the inelastic energy dissipation portion from the wall pier is larger than the corresponding portion from the BRBs. Also, there is a uniform energy dissipation in the upper levels as a result of the BRBs. On average, in the 0.1 H of the wall adjacent to the base, the energy dissipation in the SPH approach is 1.8 times the corresponding value in the EPH approach.

For each system, the contribution of wall pier sets and the whole BRBs in the inelastic energy obtained from 14 FF and 14 NF event sets has been displayed in Fig. 17. Generally, the portion of BRBs is larger than the portion of wall piers and this issue is more severe for the FF record sets. In the NF events, the contribution of wall piers to energy dissipation increases; the reason for this is the mobilization of all the structural elements (wall and BRBs) to carry the lateral force of pulse-like ground motion. In the FF events, there is no intense pulse and the portion of the wall from inelastic energy is reduced and the BRBs fulfill a greater contribution. The wall may actually be regarded as a supporting member, helping BRBs and contributing more in incoming energy dissipation in case of severe pulse-like quakes. The contribution diminishes in FF quakes.

7.4 Wall and BRB contribution for inelastic energy

On average, for all the 10-, 20- and 30-storey-EPH structures, the inelastic energy demand portion pertaining to the BRBs for NF and FF records is more than 60 and 80%, respectively. In the SPH approach, these ratios are 77 and 90% for the NF and FF events, respectively.

In the investigated systems of the current study, the design of which was according to ACI 318-11, the plastic hinge does not occur only at the RC wall base; Plasticity in the wall may in fact happen at any height. This is confirmed by some researchers for cantilever RC walls (Panagiotou and Restrepo 2009, Beiraghi and Siahpolo 2016). It is worth noting that, if a designer wants to design a wall in such a way that, in case of sever earthquakes, plasticity happens just at the base, more developed and specific methods beyond the scope of this study are needed. So in practice, EPH approach governs a wall designed according to strength method with the structural system recommended by this article, and more than about 70 percent of inelastic energy of the system is wasted through BRBs. All BRBs contribute in energy dissipation.

8. Conclusions

In this study, different energy demands for the 10-, 20- and 30-storey wall piers, coupled by BRBs, are investigated under the far-fault and near-fault earthquakes subjected to MCE level earthquakes. The systems are designed according to the current codes. For the wall piers, a single plastic hinge (SPH) approach, as well as extended plastic

hinge (EPH) approaches, are considered. NLTHA is implemented and the results show that:

- (1) On average, inelastic energy dissipation for NF records occurs in a shorter time. The accumulated dissipated inelastic energy in the equivalent velocity term during the sample FF and NF events shows that the time duration, at which almost 90% of the input inelastic energy occurs, when subjected to the FF events, is greater than about 4 times the duration at which the same percentage of the input inelastic energy occurs, when subjected to the NF events.
- (2) In almost all cases of the EPH approach, the maximum inelastic energy demand occurs around 0.3 H. In some of the wall piers, the inelastic energy dissipation in the upper region exceeds the corresponding values at the base. Furthermore, adjacent the base level, the inelastic energy dissipation portion from the wall pier is larger than the corresponding portion from the BRBs and this matter is not true for the upper levels.
- (3) For the SPH approach, in the 0.1 H adjacent to the base level that is capable to experience inelastic behavior, the inelastic energy dissipation portion from the wall pier is larger than the corresponding portion from the BRBs. On average, in the 0.1 H of the wall adjacent to the base, the energy dissipation in the SPH approach is 1.8 times the energy dissipation in corresponding area in the EPH approach. The reason is the concentration of plasticity at 0.1 H near the base of the wall in SPH approach, while in the EPH approach plasticity can extend anywhere in the wall.
- (4) Generally, for inelastic energy demand, the portion of the whole BRBs is larger than the portion of the total wall piers and this issue is more severe for the FF records. In the NF events, the contribution of wall piers to energy dissipation increases; the reason for this is the mobilization of all the structural elements (wall and BRBs) to carry the lateral force of pulse-like ground motion. The wall may actually be regarded as a supporting member, helping BRBs and contributing more in incoming energy dissipation in case of severe pulse-like quakes. The contribution diminishes in FF quakes.
- (5) On average, for all the EPH structures, the inelastic demand portion pertaining to the BRBs for the NF and FF records is more than 60 and 80%, respectively. In the SPH approach, these ratios are 77 and 90% for the NF and FF events, respectively.
- (6) In practice, EPH approach governs a wall designed according to strength method with the structural system recommended by this article. On average, more than about 70 percent of inelastic energy of the system is wasted through BRBs. All BRBs contribute in energy dissipation. It appears that utilizing the BRBs as energy dissipation members between two wall piers is an efficient concept.

References

- Abdollahzadeh, G. and Banihashemi, M. (2013), "Response modification factor of dual moment-resistant frame with buckling restrained brace (BRB)", *Steel Compos. Struct., Int. J.*, **14**(6), 621-636.
- ACI 318-11 (2011), Building code requirements for structural concrete and commentary; ACI Committee 318, Farmington Hills, MI, USA.
- ASCE/SEI 7-2010 (2010), Minimum design loads for buildings and other structures; American Society of Civil Engineers. Reston, VA, USA.
- Baker, J.W. (2007), "Quantitative classification of near-fault ground motions using wavelet analysis", *Bull. Seismol. Soc. Am.*, **97**(5), 1486-1501.
- Beiraghi, H. (2017a), "Forward directivity near-fault and far-fault ground motion effects on the responses of tall reinforced concrete walls with buckling-restrained brace outriggers", *Scientia Iranica*. DOI: 10.24200/sci.2017.4205
- Beiraghi, H. (2017b), "Earthquake effects on the energy demand of tall reinforced concrete walls with buckling-restrained brace outriggers", *Struct. Eng. Mech., Int. J.*, **63**(4), 521-536.
- Beiraghi, H. and Siahpolo, N. (2016), "Seismic assessment of RC core-wall building capable of three plastic hinges with outrigger", *Struct. Des. Tall Special Build.*, **26**(2). DOI: 10.1002/tal.1306
- Beiraghi, H., Kheyroddin, A. and Kafi, M.A. (2015), "Nonlinear fiber element analysis of a reinforced concrete shear wall subjected to earthquake records", *Transact. Civil Eng.*, **39**, 409-422.
- Beiraghi, H., Kheyroddin, A. and Kafi, M.A. (2016a), "Forward directivity near-fault and far-fault ground motion effects on the behavior of reinforced concrete wall tall buildings with one and more plastic hinges", *Struct. Des. Tall Special Build.*, **25**(11), 519-539.
- Beiraghi, H., Kheyroddin, A. and Kafi, M.A. (2016b), "Energy dissipation of tall core-wall structures with multi-plastic hinges subjected to forward directivity near-fault and far-fault earthquakes", *Struct. Des. Tall Special Build.*, **25**(15), 801-820.
- Beiraghi, H., Kheyroddin, A. and Kafi, M.A. (2016c), "Effect of record scaling on the behavior of reinforced concrete core-wall buildings subjected to near-fault and far-fault earthquakes", *Scientia Iranica*, **24**(3), p. 884.
- Bengar, H.A. and Aski, R.M. (2016), "Performance based evaluation of RC coupled shear wall system with steel coupling beam", *Steel Compos. Struct., Int. J.*, **20**(2), 337-355.
- Bernal, D. (1994), "Viscous damping in inelastic structural response", *J. Struct. Eng.*, **120**(4), 1240-1254.
- Black, C., Makris, N. and Aiken, I. (2002), "Component testing, stability analysis and characterization of buckling-restrained braces", Report No. PEER-2002/08; Pacific Earthquake Engineering Research Center, University of California, Berkeley, CA, USA.
- Bosco, M. and Marino, E.M. (2013), "Design method and behavior factor for steel frames with buckling restrained braces", *Earthq. Eng. Struct. Dyn.*, **42**(8), 1243-1263. DOI: 10.1002/eqe.2269
- CEN EC8 (2004), Design of Structures for Earthquake Resistance; European Committee for Standardization, Brussels, Belgium.
- Chopra, A.K. (2001), *Dynamics of Structures*, Prentice-Hall, NJ, USA.
- CSA Standard A23.3-04 (2005), Design of Concrete Structures; Canadian Standard Association, Rexdale, Canada.
- El-Tawil, S., Harries, K.A., Fortney, P.J., Shahrooz, B.M. and Kurama, Y. (2010), "Seismic design of hybrid coupled wall systems: State of the art", *J. Struct. Eng.*, **136**(7), 755-769.
- Fahnestock, L.A., Ricles, J.M. and Sause, R. (2007), "Experimental evaluation of a large-scale buckling-restrained braced frame", *J. Struct. Eng.*, **133**(9), 1205-1214.
- FEMA P695 (2009), Quantification of Building Seismic Performance Factors (ATC-63 Project); Federal Emergency Management Agency, Washington, D.C., USA.
- Gerami, M. and Sivandi-Pour, A. (2014), "Performance-based seismic rehabilitation of existing steel eccentric braced buildings in near fault ground motions", *Struct. Des. Tall Special Build.*, **23**(12), 881-896.
- Ghodsi, T. and Ruiz, J.A.F. (2010), "Pacific earthquake engineering research/seismic safety commission tall building design case study", *Struct. Des. Tall Special Build.*, **19**(2), 197-256.
- Harries, K.A. and McNeice, D.S. (2006), "Performance-based design of high-rise coupled wall systems", *Struct. Des. Tall Special Build.*, **15**(3), 289-306.
- Harries, K.A. and Gong, B. and Shahrooz, B.M. (2000), "Behavior and design of reinforced concrete, steel and steel-concrete coupling beams", *Earthq. Spectra*, **16**(4), 775-799.
- Jones, P. and Zareian, F. (2013), "Seismic response of a 40-storey buckling-restrained braced frame designed for the Los Angeles region", *Struct. Des. Tall Special Build.*, **22**(3), 291-299. DOI: 10.1002/tal.687
- Kalkan, E. and Kunnath, S.K. (2006), "Effects of fling-step and forward directivity on the seismic response of buildings", *Earthq. Spectra*, **22**(2), 367-390.
- Kalkan, E. and Kunnath, S.K. (2007), "Effective cyclic energy as a measure of seismic demand", *J. Earthq. Eng.*, **11**(5), 725-751.
- Kalkan, E. and Kunnath, S.K. (2008), "Relevance of absolute and relative energy content in seismic evaluation of structures", *Adv. Struct. Eng.*, **11**(1), 1-18.
- Kuwamura, H. and Galambos, T.V. (1989), "Earthquake load for structural reliability", *J. Struct. Eng., ASCE*, **115**(6), 1446-1462.
- LATBSDC (2011), An Alternative Procedure For Seismic Analysis and Design of Tall Buildings Located in the Los Angeles Region, Los Angeles Tall Buildings Structural Design Council.
- Luco, N. and Cornell, A. (2007), "Structure-specific scalar intensity measures for near source and ordinary earthquake ground motions", *Earthq. Spectra*, **23**(2), 357-392.
- Mander, J.B., Priestley, M.J.N. and Park, R. (1988), "Theoretical stress-strain model for confined concrete", *ASCE J. Struct. Eng.*, **114**(8), 1804-1826.
- Merritt, S., Uang, C.M. and Benzoni, G. (2003), Subassembly testing of star seismic buckling restrained braces; TR-2003/04, University of California at San Diego, La Jolla, CA, USA.
- Mortezaei, A. and Ronagh, H.R. (2013), "Plastic hinge length of reinforced concrete columns subjected to both far-fault and near-fault ground motions having forward directivity", *Struct. Des. Tall Special Build.*, **22**(12), 903-926.
- Nguyen, A.H., Chintanapakdee, C. and Hayashikawa, T. (2010), "Assessment of current nonlinear static procedures for seismic evaluation of BRBF buildings", *J. Constr. Steel Res.*, **66**(8-9), 1118-1127.
- NZS 3101 (2006), New Zealand Standard, Part 1—The Design of Concrete Structures; Standards New Zealand, Wellington, New Zealand.
- Orakcal, K. and Wallace, J.W. (2006), "Flexural Modeling of reinforced Concrete Walls-Experimental Verification", *ACI Struct. J.*, **103**(2), 196-206.
- Palmer, K.D., Christopoulos, A.S., Lehman, D.E. and Roeder, C.W. (2014), "Experimental evaluation of cyclically loaded, large-scale, planar and 3-d buckling-restrained braced frames", *J. Constr. Steel Res.*, **101**, 415-425.
- Panagiotou, M. and Restrepo, J. (2009), "Dual-plastic hinge design concept for reducing higher-mode effects on high-rise cantilever wall buildings", *Earthq. Eng. Struct. Dyn.*, **38**(12), 1359-1380.

- Paulay, T. and Priestley, M.J.N. (1992), *Seismic Design of Reinforced Concrete and Masonry Buildings*, Wiley, Hoboken, NJ, USA.
- PERFORM-3D (2006), *Nonlinear Analysis and Performance Assessment for 3D Structures; V.4, User Guide*, Computers and Structures, Inc., Berkeley, CA, USA.
- PERFORM-3D (2011), *Nonlinear Analysis and Performance Assessment for 3D Structures; V.4.0.3*, Computers and Structures, Inc., Berkeley, CA, USA.
- Powell, G. (2007), "Detailed example of a tall shear wall building using CSI's Perform 3D nonlinear dynamic analysis", Computers and Structures Inc., Berkeley, CA, USA.
- Priestley, M.J.N. and Grant, D.N. (2005), "Viscous damping in seismic design and analysis", *J. Earthq. Eng.*, **9**(SP2), 229-255.
- Sahoo, D.R. and Chao, S. (2010), "Performance-based plastic design method for buckling-restrained braced frames", *Eng. Struct.*, **32**(9), 2950-2958.
- Shargh, F.H. and Hosseini, M. (2011), "An optimal distribution of stiffness over the height of shear buildings to minimize the seismic input energy", *J. Seismol. Earthq. Eng.*, **13**(1), 25-32.
- Simpson, Gumpertz & Heger, Inc. (2009), *Detailed Design Write up for BRBF building*, Simpson, Gumpertz & Heger, Inc., San Francisco, CA, USA.
- Sivandi-Pour, A., Gerami, M. and Kheyroddin, A. (2015), "Determination of modal damping ratios for non-classically damped rehabilitated steel structures. Iranian Journal of Science and Technology", *Transact. Civil Eng.*, **39**(C1), p. 81.
- Somerville, P. (1997), "The characteristics and quantification of near-fault ground motion", *Proceedings of the FHWA/NCEER Workshop on the National Representation of Seismic Ground Motion for New and Existing Highway Facilities*, Burlingame, CA, USA, May.
- Stewart, J.P., Chiou, S.J., Bray, J.D., Graves, R.W., Somerville, P.G. and Abrahamson, N.A. (2001), "Ground motion evaluation procedures for performance based design", PEER 2001-09; Pacific Earthquake Engineering Research Center, University of California at Berkeley, Berkeley, CA, USA.
- Tsai, K.-C. and Hsiao, P.-C. (2008), "Pseudo-dynamic test of a full-scale CFT/BRB frame—Part II: Seismic performance of buckling-restrained braces and connections", *Earthq. Eng. Struct. Dyn.*, **37**(7), pp. 1099-1115.
- Tsai, K.-C., Hsiao, P.-C., Wang, K.-J., Weng, Y.-T., Lin, M.-L., Lin, K.-C., Chen, C.-H., Lai, J.-W. and Lin, S.-L. (2008), "Pseudo-dynamic tests of a full-scale CFT/BRB frame—Part I: Specimen design, experiment and analysis", *Earthq. Eng. Struct. Dyn.*, **37**(7), 1081-1098.
- Uang, C.M. and Bertero, V.V. (1997), "Seismic response of an instrumented 13-story steel frame building damaged in the 1994 Northridge earthquake", *Earthq. Spectra*, **13**(1), 131-148.
- Watanabe, A. (1992), "Development of composite brace with a large ductility", *Proceedings of the U.S.-Japan Workshop on Composite and Hybrid Structures*, (Goel S. and Yamanouchi, H. Ed.), Berkeley, CA, USA, September.